Benchmarking high-field few-electron correlation and QED contributions in Hg^{75+} to Hg^{78+} ions. II. Theory

Z. Harman,[1] I. I. Tupitsyn,[1,2] A. N. Artemyev,[1,2] U. D. Jentschura,[1] C. H. Keitel,[1] J. R. Crespo López-Urrutia,[1] A. J. González Martínez,[1] H. Tawara,[1] and J. Ullrich[1]

[1]*Max-Planck-Institut für Kernphysik, Saupfercheckweg 1, 69117 Heidelberg, Germany*

[2]*Department of Physics, St. Petersburg State University, Oulianovskaya 1, Petrodvorets, 198504 St. Petersburg, Russia*

(Received 6 February 2006; published 23 May 2006)

Theoretical resonance energies for *KLL* dielectronic recombination into He-, Li-, Be-, and B-like Hg ions are calculated by various means and discussed in detail. We apply the multiconfiguration Dirac-Fock and the configuration interaction Dirac-Fock-Sturmian methods, and quantum electrodynamic many-body theory. The different contributions such as relativistic electron interaction, quantum electrodynamic contributions, and finite nuclear size and mass corrections are calculated and their respective theoretical uncertainties are estimated. Our final results are compared to experimental data from the preceding paper. The comparison of theoretical values with the experimental energies shows a good overall agreement for most transitions and illustrates the significance of relativistic electron interaction contributions including correlation, magnetic, and retardation effects and quantum electrodynamic corrections. A few discrepancies found in specific recombination resonances for initially Li- and Be-like Hg ions are pointed out, suggesting the need for further theoretical and experimental studies along these isoelectronic sequences.

DOI: 10.1103/PhysRevA.73.052711 PACS number(s): 34.80.Lx, 31.30.Jv, 31.15.Ne, 31.15.Md

I. INTRODUCTION

Over the last two decades, the theoretical and experimental progress in investigations of highly charged ions has opened perspectives for probing relativistic, quantum electrodynamic (QED), electron interaction, and nuclear effects in strong binding fields (see, e.g., Refs. [1,2]). As the relative importance of relativistic and radiative corrections increases with high powers of the nuclear charge Z, very heavy, few-electron ions provide a unique testing ground for advanced atomic structure theories. Moreover, as the charge state of the ions can be directly selected in modern experimental environments provided by electron beam ion traps (EBITs), an additional degree of experimental freedom is available which can be used to address the influence of relativistic correlation effects.

Due to experimental difficulties in producing such very heavy few-electron ions, there exist only a few measurements for the heaviest elements with nuclear charge number exceeding $Z=80$. The energy of the $2s_{1/2}$-$2p_{3/2}$ excitation, for example, was determined with high precision in Li-like Bi [3], and the $2s_{1/2}$-$2p_{1/2}$ transition energy in Li-like Au, Pb, and U ions at the GSI experimental storage ring [4]. Very recently, the energy of the same transition in U^{89+} was determined at the EBIT of the Lawrence Livermore National Laboratory with a 50 ppm accuracy, allowing the testing of bound-state QED theory on the two-loop level [5].

In this paper, we study the dynamical process of dielectronic recombination (DR) as a means of generating and studying excited ions in an electron beam ion trap. In the first step of DR, a free electron is captured into an ion by the simultaneous excitation of a bound electron as illustrated in Fig. 1 for the case of *KLL* DR into initially He-like ions. For ions of different charge states (initially Li-, Be-, and B-like), this scheme differs only in the number of spectator electrons in the L shell. The resolving power of our experiment allows us to separate peaks corresponding to different charge states and electronic states. The designation *KLL* refers to the shell structure of the bound electronic states actively involved in the process. In the second step of DR, the excited autoionizing state d decays radiatively to a bound final state f. The energy E_{res} of the free electron at resonance fulfills the following energy conservation condition: $E_{\mathrm{res}}+E_i=E_d$, with E_i being the energy of the initial ionic N-electron bound state and E_d the energy of the excited intermediate $(N+1)$-electron state. This energy can be determined in DR measurements as the position of the resonance peak, yielding spectroscopic information. DR experiments performed with ion storage rings [6,7] or ion traps [8–10] have proved to be a useful tool to provide new insight into the structure of excited atomic states and the correlated relativistic dynamics in electron recombination processes. For very low-lying resonances associated with inner-shell transitions, the experimental resolution in storage rings is sufficient to determine hyperfine splitting constants [11]. When the photons emitted after the resonant recombination are detected, e.g., as in an EBIT

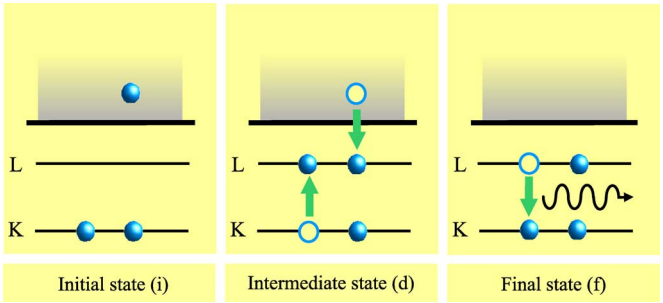

FIG. 1. (Color online) Schematic representation of *KLL* dielectronic recombination into He-like ions.

measurement, the x-ray energies $E_x = E_d - E_f$ can also be determined simultaneously. Our experiment, performed recently at the Heidelberg EBIT facility, is discussed in detail in the companion paper [12] (see also Ref. [13]). In the present paper, we describe in more detail the theoretical approaches applied to calculate resonance energies.

In contrast to singly excited states, autoionizing states involved in DR are more challenging for theoretical predictions. With at least two electrons in the L shell, electron interaction effects to the energy become more pronounced than for K-shell electrons confined by the strongest nuclear Coulomb fields. Configuration mixing in the open shells intertwined with fine-structure splitting requires advanced theoretical methods capable of accurately describing relativistic correlation effects. Furthermore, especially in high-Z ions such as Hg which is studied here, such states are more influenced by magnetic and retardation corrections to the electron-electron interaction. Since in *KLL* processes a $1s$ electron is excited to a higher orbital, these resonance transition energies are also very sensitive to QED contributions.

We applied the following theoretical models to the calculation of electron correlation contributions to atomic energy levels in relativistic many-electron systems: (*i*) the multiconfiguration Dirac-Fock (MCDF) method [14–19], (*ii*) the configuration interaction Dirac-Fock-Sturmian (CI-DFS) method, and (*iii*) the quantum electrodynamic many-body (QMB) theory. We cover *KLL* DR resonance energies for Hg ions of initial charge states ranging from He-to B-like. The MCDF method was applied previously to calculate DR resonance energies and cross sections in very heavy few-electron ions, e.g., for *KLL* transitions [20,21], and for recombination into high Rydberg states with a simultaneous intrashell excitation of the Li-like ionic core [4,22]. We have made an attempt at determining not only a theoretical value, but also a theoretical uncertainty associated to our results (Table XVI), in order to make a quantitative comparison of experiment and theory possible. In the literature on the theory of many-electron systems, such uncertainty estimates are sometimes lacking, but we found them indispensable for a meaningful interpretation of the current high-precision study. We do not claim a rigorous derivation of the theoretical errors but we rather estimate them as an orientation by considering the dependence of contributions on system parameters or the spread of the results for different methods.

This article is organized as follows: in Sec. II, we summarize the theoretical models applied. In Sec. III, our approach to radiative and nuclear recoil corrections is described. This part is followed by the presentation and analysis of our numerical results in comparison with experimental data (Sec. IV). In Sec. V, we finally conclude with a summary. Atomic units are used throughout this paper and energies are measured from the rest energy $m_e c^2 \equiv c^2$ of the free electron, in units of eV unless stated otherwise.

II. CALCULATION OF RELATIVISTIC ELECTRON INTERACTION CONTRIBUTIONS

For the evaluation of relativistic electron-electron interaction contributions we start with the Dirac-Coulomb-Breit (DCB) Hamiltonian of an atom or ion with N electrons given by

$$H^{\mathrm{DCB}}(\omega) = \sum_{i=1}^{N} h_i + \sum_{i<j}^{N} V_{ij}(\omega). \tag{1}$$

Here, the one-particle operators are

$$h_i = c\,\boldsymbol{\alpha}_i \cdot \mathbf{p}_i + (\beta_i - 1)c^2 + V_{\mathrm{nuc}}(r_i), \tag{2}$$

where the indices i and j enumerate the electrons and c is the speed of light in vacuum. [The index i is not subjected to the Einstein summation convention in Eq. (2).] The vector operator $\mathbf{p}_i$ is the relativistic momentum operator and $\boldsymbol{\alpha}_i$ and β_i are the Dirac matrices acting on the four-component wave function of the ith particle. The nuclear model potential V_{nuc} is chosen to correspond to a two-parameter Fermi charge distribution (for details see below).

In the Coulomb gauge the electron-electron interaction operator V_{ij} is given as the sum of the Coulomb and Breit terms:

$$V_{ij}(\omega) = V_{ij}^{C} + V_{ij}^{B}(\omega), \tag{3}$$

with $V_{ij}^{C} = 1/r_{ij}$ and r_{ij} being the distance between two particles. The frequency-dependent Breit interaction $V_{ij}^{B}(\omega)$ can be decomposed into the following parts:

$$V_{ij}^{B}(\omega) = V_{ij}^{\mathrm{magn}} + V_{ij}^{\mathrm{ret}} + V_{ij}^{\mathrm{ret}}(\omega). \tag{4}$$

Here, the magnetic (Gaunt) term is given by

$$V_{ij}^{\mathrm{magn}} = -\frac{\boldsymbol{\alpha}_i \cdot \boldsymbol{\alpha}_i}{r_{ij}}, \tag{5}$$

and the retardation of the scalar and the transverse interaction in the Breit approximation is

$$V_{ij}^{\mathrm{ret}} = \frac{\boldsymbol{\alpha}_i \cdot \boldsymbol{\alpha}_j}{2r_{ij}} - \frac{(\boldsymbol{\alpha}_i \cdot \mathbf{r}_{ij})(\boldsymbol{\alpha}_j \cdot \mathbf{r}_{ij})}{2r_{ij}^3}. \tag{6}$$

The sum of V_{ij}^{magn} and V_{ij}^{ret} is the usual Breit interaction V_{ij}^{B}. Additional retardation effects are described by the term depending on the frequency of the exchanged transverse photon ω:

$$V_{ij}^{\mathrm{ret}}(\omega) = -\,\boldsymbol{\alpha}_i \cdot \boldsymbol{\alpha}_j \frac{\cos(\omega r_{ij}) - 1}{r_{ij}} + (\boldsymbol{\alpha}_i \cdot \boldsymbol{\nabla}_i)(\boldsymbol{\alpha}_j \cdot \boldsymbol{\nabla}_j) \frac{\cos(\omega r_{ij}) - 1 + \omega^2 r_{ij}^2/2}{\omega^2 r_{ij}}. \tag{7}$$

Here, $\boldsymbol{\nabla}_i$ denotes differentiation with respect to the position vector of the ith electron. (We reemphasize that the Einstein summation convention is not adopted in this work.) The total interaction operator in Eq. (3)can be derived in a quantum electrodynamic framework from the exchange of a virtual photon between the electrons, including all components of the photon propagator. Magnetic and retardation interactions are mandatory to take into account when calculating structural properties of high-Z ions, especially when inner-shell electrons are involved as in our case.

A. Multiconfiguration self-consistent field methods

In multiconfiguration methods, the many-electron atomic state function (ASF) ansatz is given as a linear superposition of configuration state functions (CSFs) sharing common total angular momentum (J), magnetic (M), and parity (P) quantum numbers [16]:

$$|\Gamma PJM\rangle = \sum_{k=1}^{n_c} c_k |\gamma_k PJM\rangle. \tag{8}$$

The CSFs $|\gamma_k PJM\rangle$ are constructed as jj-coupled N-particle Slater determinants of one electron wave functions. In Eq. (8), γ_k is a multi-index that includes all the information needed to fully describe the CSF, which includes orbital occupation and coupling of one-electron angular momenta. The number of CSFs is denoted by n_c. Γ collectively denotes all the γ_k included in the representation of the ASF. The (single-configuration) Dirac-Fock (DF) method consists of applying only the leading ($k=1$)-term in the configuration expansion (8). In multiconfiguration methods, electron correlation contributions are accounted for by adding configurations of the same symmetry.

The quantum numbers for the one-particle wave functions are the principal quantum number n, the angular momentum (orbital+spin) $j=|\kappa|-\frac{1}{2}$ and its projection μ:

$$\phi_{n\kappa\mu}(\mathbf{r}) = \frac{1}{r}\begin{pmatrix} P_{n\kappa}(r)\Omega_{\kappa\mu}(\hat{r}) \\ iQ_{n\kappa}(r)\Omega_{-\kappa\mu}(\hat{r}) \end{pmatrix}. \tag{9}$$

In the above expression, $\kappa=2(l-j)(j+1/2)$ is the relativistic angular momentum quantum number, $P_{n\kappa}(r)$ and $Q_{n\kappa}(r)$ are the radial parts of the large and small component wave functions to be determined, and $\Omega_{\kappa\mu}(\hat{r})$ is the spinor spherical harmonic in the lsj coupling scheme with argument $\hat{r}$ representing the unit position vector [14].

1. The multiconfiguration Dirac-Fock method

In our MCDF and CI-DFS calculations, the Coulomb part of the interaction is treated self-consistently, i.e., the eigenvalues and eigenvectors of the Dirac-Coulomb Hamiltonian

$$H^{\mathrm{DC}} = \sum_{i=1}^{N} h_i + \sum_{i<j}^{N} V_{ij}^{C} \tag{10}$$

are approximated. According to the Rayleigh-Ritz variational principle, a state function is an eigenstate of the Hamiltonian H^{DC} if and only if the energy functional defined as the expectation value of H^{DC} is left unchanged for any infinitesimal variation of the wave function. Considering the ansatz (8)with a given set of one-electron orbitals and CSFs, the mixing coefficients can be determined by diagonalizing the Hamiltonian with the given basis set, i.e., the configuration expansion coefficients c_l are solutions of the matrix equation

$$\sum_{l=1}^{n_c} (\langle \gamma_k PJM|H^{\mathrm{DC}}|\gamma_l PJM\rangle - E_{\Gamma}^{\mathrm{DC}}\delta_{kl})c_l = 0. \tag{11}$$

This approach, with the wave functions kept fixed, leads to the configuration interaction method (CI). Furthermore, if the variation of the orbital wave functions is also allowed, one obtains the MCDF optimal level method. Applying the variational principle, the following set of MCDF equations for the radial wave functions can be derived [18]:

$$\left(\frac{d}{dr} + \frac{\kappa_a}{r}\right)P_{n_a\kappa_a}(r) - \left(2c - \frac{\epsilon_a}{c} + \frac{Y_a(r)}{cr}\right)Q_{n_a\kappa_a}(r) = -\frac{\chi_a^P(r)}{r}, \tag{12a}$$

$$\left(\frac{d}{dr} - \frac{\kappa_a}{r}\right)Q_{n_a\kappa_a}(r) + \left(-\frac{\epsilon_a}{c} + \frac{Y_a(r)}{cr}\right)P_{n_a\kappa_a}(r) = \frac{\chi_a^Q(r)}{r}. \tag{12b}$$

Here, a is the index for a given subshell orbital. These equations are coupled to each other through the direct (Y_a) and the exchange (χ_a^P, χ_a^Q) potentials [18]. Only the direct potential contains the Coulomb field of the nucleus, whereas both the direct as well as the exchange potentials contain contributions from the electrostatic potential induced by the other electrons, and therefore include integrals of the electronic orbitals. The integro-differential Eqs. (12a) and (12b)are solved iteratively together with the algebraic equations (11)until self-consistency is reached for the radial wave functions and for the mixing coefficients c_l. In the (single-configuration) DF case, the mean field potential is spherically symmetric and Eqs. (12a) and (12b)may be regarded as eigenvalue equations for the DF operator h^{DF}. For more details on the MCDF method, we refer to the articles [14–19].

We use the GRASP92 [19](General-Purpose Relativistic Atomic Structure Program) package to perform the numerical task of solving the multiconfiguration Dirac-Fock Eqs. (12a) and (12b). In our calculations, the active space of CSFs includes all single and double excitations from the reference configurations up to one-particle orbitals in the $n=3$ shell. This leads to 14, 30, 38, and 168 jj-coupled relativistic CSFs for He-, Li-, Be-, and B-like ground states, respectively, and typically a few hundred (41 to 742) configurations for autoionizing states.

We were able to reach convergence in the self-consistent calculations with virtual excitations into all orbitals with $n \leqslant 3$. The employed set of CSFs provided sufficient convergence of the correlation energy. Indeed, the accuracy reached with a given set of CSFs was estimated by observing the apparent rate of convergence of the energies as the configuration basis set was increased. A comparison to other, related approaches (e.g., the Dirac-Fock-Sturmian method to be discussed below) was made in order to check the consistency of the final result as well as of the uncertainty estimates thus obtained. We note that our configuration truncation errors are smaller than the uncertainty due to self-energy screening contributions (see also Sec. IIIbelow).

After the application of the MCDF method to solve the correlated relativistic Coulomb problem, the long-wavelength ($\omega \to 0$) Breit interaction corrections are included by a CI method. Matrix elements of the Breit interaction operator V^B are calculated with wave functions generated by the Coulomb self-consistent method and added to the Dirac-Coulomb Hamiltonian matrix, and the resulting

TABLE I. Natural abundances, nuclear spin (I) and parity (π) quantum numbers, RMS nuclear charge radii (from Ref. [27]), and atomic masses (from Refs. [28,29]) of Hg isotopes used in the calculations.

A	Abundance (%)	$I\pi$	R_{RMS} (fm)	Atomic mass (amu)
196	0.15	0+	5.4388	195.965 833
198	9.97	0+	5.4466	197.966 769 0
199	16.87	1/2−	5.4484	198.968 279 9
200	23.10	0+	5.4549	199.968 326 0
201	13.18	3/2−	5.4583	200.970 302 3
202	29.86	0+	5.4633	201.970 643 0
204	6.87	0+	5.4742	203.973 493 9

matrix is rediagonalized. Within this approach, the effect of the magnetic and Breit retardation terms is included in the configuration mixing coefficients (but not in the radial wave functions).

The frequency-dependent part (7)of the electron-electron interaction operator is calculated in the first order of perturbation theory with approximate Dirac-Coulomb eigenfunctions. In the framework of Hamiltonian methods, it is not self-consistent to evaluate higher-than-first-order corrections due to the frequency-dependent retardation.

2. The configuration interaction Dirac-Fock-Sturmian method

Another generalization of the single-configuration DF scheme to describe correlation effects can be achieved in the framework of the configuration interaction Dirac-Fock-Sturmian method. The CI-DFS method has been applied successfully to calculate, for example, the wavelength [23], lifetime [24,25], and isotope shift [26]of forbidden M1 transitions in Be- and B-like Ar ions. Within this method, the occupied orbitals, denoted by ϕ_{a_0}, are obtained first by the DF procedure. The vacant correlation orbitals $\tilde{\phi}_a$ are determined by numerically solving the Dirac-Fock-Sturmian equations

$$[h^{\mathrm{DF}} - \epsilon_{a_0}]\tilde{\phi}_a(\mathbf{r}) = \xi_a W(r)\tilde{\phi}_a(\mathbf{r}), \tag{13}$$

where h^{DF} is the one-particle Dirac-Fock operator containing the spherical mean field potential, ϵ_{a_0} is the one-electron energy of the occupied DF orbital ϕ_{a_0}, and $W(r)$ is a weight function possessing a constant sign for all values of r. The parameter ξ_a can be regarded as an eigenvalue of the Sturmian operator. With the choice $W(r)\to 0$ for $r\to\infty$, all Sturmian functions $\tilde{\phi}_a$ have the same asymptotics as their $W=0$ Dirac-Fock counterparts at large values of r. For $\xi_a=0$, the Sturmian function coincides with the reference DF orbital ϕ_{a_0}. In our calculations, the weight function

$$W(r) = \frac{1 - e^{-(\gamma r)^2}}{(\gamma r)^2} \tag{14}$$

was found to be numerically effective. Here, γ is an adjustable parameter. In contrast to the choice $W(r)=1/r$ widely used in the nonrelativistic case, the function (14)is regular at the origin. The Sturmian operator is Hermitian and, in contrast to the Fock operator, its spectrum does not contain a continuous part, which facilitates the numerical treatment of the continuum. Still, the discrete set of Sturmian functions forms a complete basis set of one-electron wave functions, which makes the method a convenient tool for the evaluation of correlation corrections to many-electron states. The completeness of the DFS basis was tested numerically in Ref. [25]by reproducing hydrogenic wave functions.

We use all configuration state functions generated by single and double excitations from occupied orbitals up to $n=9$ shells (for states formed by DR into initially He-, Li-, and Be-like ions) and up to $n=6$ for B-like ions, and part of the triple excitations up to the $4f$ orbital. It should be stressed that, as a consequence of the conceptually different method, the computer code used in the CI-DFS approach is completely different from the one used for the MCDF results, giving us the possibility to numerically cross-check the

TABLE II. An example of finite nuclear size (FNS) contributions to the He-like initial and $1s2s^2$ intermediate state level energies E_i, E_d and to the resonance energy $E_{\mathrm{res}}=E_d-E_i$ for Hg ions with $A=202$ (units are eV). See text for explanations.

Contribution	E_i	E_d	E_{res}
One-electron FNS	109.3	72.0	−36.1
DF correction to the FNS effect	−1.2	−1.3	−0.1

TABLE III. An example of various Coulomb electron-electron interaction contributions to the He-like initial and $1s2s^2$ intermediate state level energies E_i, E_d and to the resonance energy $E_{\mathrm{res}}=E_d-E_i$ for a pointlike Hg nucleus (units are eV). See text for explanations.

Contribution	E_i	E_d	E_{res}
Sum of one-electron Schrödinger energies	−174 152.9	−130 614.7	43 538.2
HF correction	1 357.6	1 187.4	−170.2
MCHF nonrelativistic correlation	−1.3	−37.1	−35.7
Sum of one-electron Dirac energies	−192 231.8	−145 360.2	46 871.5
DF correction	1 576.6	1 402.6	−173.9
MCDF relativistic correlation	−1.2	−16.3	−15.1

TABLE IV. Coulomb and Breit contributions to the level energy of the ground and autoionizing states involved in the dielectronic recombination processes for initially He-like Hg ions (units are eV).

	V^C		V^B		$V^{\rm ret}(\omega)$	
State	MCDF	CI-DFS	MCDF	CI-DFS	MCDF	CI-DFS
$[1s^2]_0$	−190 548.3(0.4)	−190 548.48(2)	202.9(1.5)	203.61(3)	0.00(10)	0.00(10)
$[1s2s^2]_{1/2}$	−143 901.8(0.6)	−143 902.1(3)	25.4(0.8)	25.4(2)	0.35(10)	0.33(10)
$[(1s2s)_0 2p_{1/2}]_{1/2}$	−143 674.4(1.6)	−143 674.8(3)	74.3(1.2)	73.9(2)	0.36(10)	0.40(10)
$[(1s2p_{1/2})_0 2p_{3/2}]_{3/2}$	−141 422.4(1.6)	−141 422.8(1)	50.9(1.1)	50.5(1)	−2.09(10)	−2.04(10)
$[(1s2s)_0 2p_{3/2}]_{3/2}$	−141 325.7(1.2)	−141 326.0(3)	59.1(0.5)	59.1(1)	0.65(10)	0.61(10)
$[1s(2p_{3/2})_2^2]_{5/2}$	−139 139.3(0.8)	−139 140.0(5)	14.4(0.5)	14.6(4)	−5.69(10)	−5.66(10)

electron interaction contributions determined by these two methods.

In the CI-DFS method we explicitly apply the no-pair approximation, in which only one-particle eigenstates with positive energy are taken into account, i.e., the solutions of the Hamiltonian

$$H^{\rm np} = \Lambda^+ H^{\rm DC} \Lambda^+ \tag{15}$$

are determined. The operator Λ^+ projects onto positive-energy Dirac eigenstates. As the electron interaction contributions calculated by means of this method agree well with the results of the MCDF theory where such projection operators were not introduced (see the following subsection), we assume the contribution due to negative-energy states to be negligible at the present level of accuracy.

The Breit interaction contributions are calculated in the same way as described in the case of the MCDF method.

3. Numerical results for electron interaction contributions

In high-Z atoms, the electron distributions and thus the energy levels are sensitive to nuclear finite-size effects. Throughout this article, we use the Fermi two-parameter distribution for describing the charge distribution of the considered nuclei,

$$\rho_{\rm nuc}(r) = \frac{\rho_0}{1 + e^{(r-\bar{c})/a}}, \quad a = t4\ln 3. \tag{16}$$

Here, $\bar{c}$ is the half-charge radius, the value of r for which $\rho_{\rm nuc}(r) = \frac{1}{2}\rho_0$, and t is the skin thickness parameter. The experimental measurements were performed using naturally abundant Hg isotopes. We use root-mean-square (RMS) radii for all isotopes taken from Ref. [27]. The natural isotopic abundances and RMS radii are listed in Table I, together with accurate atomic masses taken from Refs. [28,29].

As an example, finite nuclear size (FNS) contributions are presented in Table IIfor the case of the $1s^2 \rightarrow 1s2s^2$ excitation (by dielectronic recombination). In the first row of the table, the sum of one-electron FNS contributions is given in the independent-particle approximation. The inclusion of the DF electron interaction introduces a contribution of roughly −1.2 eV for both the initial and the excited states, as can be seen in the second row. However, these terms largely cancel in the calculation of the resonance energy. Correlation corrections to the FNS effects are found to be negligible on the present level of experimental accuracy. The presence of different isotopes in the present EBIT measurement introduces a spread of ±(0.3–0.4) eV of the resonance energies, depending on the orbital occupation of the *KLL* autoionizing states.

Table IIIillustrates the role of relativistic Coulomb correlation for the $1s2s^2$ resonant state formed after dielectronic recombination into He-like mercury. Listed are the nonrela-

TABLE V. Coulomb and Breit contributions to the level energy of the ground and autoionizing states involved in the dielectronic recombination processes for initially Li-like Hg ions (units are eV).

	V^C		V^B		$V^{\rm ret}(\omega)$	
State	MCDF	CI-DFS	MCDF	CI-DFS	MCDF	CI-DFS
$[1s^2 2s]_{1/2}$	−214 140.5(0.6)	−214 140.51(4)	222.4(1.8)	224.16(4)	0.33(10)	0.34(10)
$[1s2s^2 2p_{1/2}]_1$	−167 126.4(0.6)	−167 126.6(2)	28.7(1.1)	29.75(3)	0.32(10)	0.32(10)
$[((1s2s)_1 2p_{1/2})_{3/2} 2p_{3/2}]_2$	−164 723.1(4.0)	−164 727.2(3)	33.8(2.9)	31.0(2)	−0.35(12)	−0.29(12)
$[((1s2s)_1 2p_{1/2})_{3/2} 2p_{3/2}]_1$	−164 681.8(4.0)	−164 685.1(2)	39.9(2.3)	38.00(4)	1.07(13)	1.13(13)
$[((1s2s)_0 2p_{1/2})_{1/2} 2p_{3/2}]_2$	−164 621.5(1.0)	−164 622.1(8)	73.6(1.9)	73.3(5)	−1.35(10)	−1.34(10)
$[((1s2s)_1 2p_{1/2})_{3/2} 2p_{3/2}]_3$	−164 795.1(2.5)	−164 798.0(1.0)	3.5(0.2)	3.5(2)	−3.37(10)	−3.37(10)
$[(1s2s)_1 (2p_{3/2})_2^2]_3$	−162 622.9(1.2)	−162 623.0(4)	15.9(0.2)	15.8(2)	−5.45(10)	−5.45(10)

TABLE VI. Coulomb and Breit contributions to the level energy of the ground and autoionizing states involved in the dielectronic recombination processes for initially Be-like Hg ions (units are eV).

	V^C		V^B		$V^{\mathrm{ret}}(\omega)$	
State	MCDF	CI-DFS	MCDF	CI-DFS	MCDF	CI-DFS
$[1s^22s^2]_0$	−237 370.6(1.4)	−237 371.17(6)	248.5(0.6)	248.86(4)	0.64(10)	0.65(10)
$[1s2s^2(2p_{1/2})^2]_{1/2}$	−189 917.1(1.5)	−189 918.1(1)	83.8(1.1)	84.15(3)	0.30(10)	0.29(10)
$[(1s2s^22p_{1/2})_1 2p_{3/2}]_{3/2}$	−187 789.1(1.1)	−187 790.0(1)	82.0(1.4)	81.5(1)	−2.29(10)	−2.26(10)
$[(1s2s^22p_{1/2})_0 2p_{3/2}]_{3/2}$	−187 713.8(2.1)	−187 714.8(3)	89.5(0.8)	89.8(1)	1.00(10)	0.95(10)
$[(1s2s^22p_{1/2})_1 2p_{3/2}]_{5/2}$	−187 748.4(2.6)	−187 749.4(2.4)	35.3(0.5)	35.7(8)	−3.07(10)	−3.08(10)
$[1s2s^2(2p_{3/2})^2_2]_{5/2}$	−185 583.6(2.0)	−185 584.95(4)	47.3(0.5)	46.93(3)	−5.22(10)	−5.21(10)

tivistic Hartree-Fock contribution, the nonrelativistic correlation energy determined by an MCHF method, and their relativistic counterparts both for the initial two-electron ground state as well as for the excited three-electron state. The "nonrelativistic" results are calculated by setting the velocity of light 10^5 times larger than its actual physical value in the relativistic computer codes. The correlation correction is especially important for the excited state. It has a value of −37.1 eV in the nonrelativistic case, but decreases to −16.3 eV when relativity is taken into account, which demonstrates the importance of the relativistic treatment of electron correlation.

Tables IV–VIIshow the Coulomb and Breit contributions to the level energy of the ground states and autoionizing states involved in the dielectronic recombination processes for initially He-, Li-, Be-, and B-like Hg ions, respectively. The error of the Coulomb interaction calculations is determined by analyzing the convergence of correlation energy when extending the size of the configuration set applied. In the case of the CI-DFS method, the error of the Coulomb interaction energy is estimated by taking the difference of the values achieved using a large CSF set with virtual excitations up to $n=9$ and $n=6$. (In the case of autoionizing states formed by DR into B-like Hg, the difference of the $n=6$ and $n=3$ results is taken.) For the MCDF method, the configuration set contains orbitals from $1s$ to $3d$ and the error is determined as the difference of the results for $n=3$ and $n=2$, leading to relatively larger error bars. A similar estimation procedure is used for the frequency-independent part of the Breit interaction.

As both SCF methods yield an approximate value only for the frequency dependence of the Breit retardation term beyond the DF- or single-configuration approximation, the error of this term is determined by taking the difference of the results of the two approaches and multiplying this by a factor of 2 and rounding up to yield at least 0.1 eV.

B. Quantum electrodynamic many-body theory

While the methods described previously start from the the Dirac-Coulomb-Breit many-electron Hamiltonian (1), the quantum electrodynamic many-body theory (QMB) starts from the *ab initio* QED description of the many-electron system in the Furry picture. This approach allows the systematic treatment of radiative corrections.

Unfortunately, the factorial growth of the number of the diagrams with the number of electrons limits the practical applicability of the method. Traditionally, this method is applied to the theoretical investigation of the low-lying energy levels of one-, two-, and three-electron systems (see, e.g., Refs. [30,31]and references therein). The present calculation is the first attempt to apply this method to a wider range of systems including doubly excited states with a relatively large number of electrons.

In the present work, we have used noninteracting electronic wave functions in the field of the nucleus as the initial approximation. The interelectronic interaction and QED effects have been taken into account using standard perturbation theory and Feynman diagram techniques [32]. The electron-electron interaction terms are calculated in the following way: the first-order correction (one-photon exchange diagram) has been evaluated in a rigorous field-theoretical framework, taking into account the frequency dependence of the photon propagator. This corresponds to evaluating the matrix element of the total interaction operator (3)on the zeroth-order state functions. The second-order correction

TABLE VII. Coulomb and Breit contributions to the level energy of the ground and autoionizing states involved in the dielectronic recombination processes for initially B-like Hg ions (units are eV).

	V^C		V^B		$V^{\mathrm{ret}}(\omega)$	
State	MCDF	CI-DFS	MCDF	CI-DFS	MCDF	CI-DFS
$[1s^22s^22p_{1/2}]_{1/2}$	−259 991.8(2.2)	−259 993.2(1.5)	294.0(2.5)	292.7(0.4)	0.74(21)	0.63(21)
$[1s2s^2(2p_{1/2})^2 2p_{3/2}]_1$	−210 101.0(3.1)	−210 103.3(3.5)	106.0(1.8)	104.4(1.0)	1.72(10)	1.72(10)
$[1s2s^2(2p_{1/2})^2 2p_{3/2}]_2$	−210 144.7(4.2)	−210 146.2(3.6)	94.9(1.5)	94.2(0.9)	−3.06(10)	−3.07(10)
$[(1s2s^22p_{1/2})_1(2p_{3/2})^2_2]_3$	−207 990.2(3.6)	−207 990.4(3.9)	48.4(1.1)	48.3(0.7)	−5.16(10)	−5.17(10)

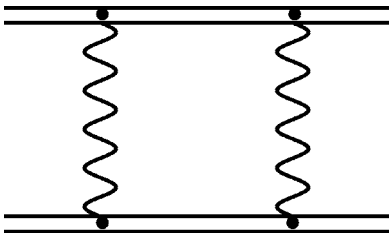

FIG. 2. Feynman diagram representing the exchange of two photons between two electrons (ladder diagram). Double lines indicate electrons propagating in the Coulomb field of the nucleus.

(two-photon exchange diagram, depicted in Fig. 2) has been calculated using the relativistic many-body perturbation theory (RMBPT) approximation, i.e., neglecting higher-order retardation effects, crossed-photon terms, and the virtual creation of electron-positron pairs [31].

Technically, the calculation has been performed using the *B*-spline method for the generation of the quasi-complete system of the Dirac equation solutions [33]. The details of the application of this method to the QED calculations can be found in Ref. [31].

The fast growth of the number of the diagrams is not the only limitation for the application of the QMB method to the theoretical investigation of many-electron systems. The increase of the number of electrons also leads to the necessity of taking into account the interelectronic interaction in a more accurate way. This problem can be solved by the inclusion of the spherically averaged part of the interelectronic interaction in the zeroth-order Hamiltonian. More accurate results can be achieved in future calculations by a combination of the QMB approach and the CI-DFS method.

III. QUANTUM ELECTRODYNAMIC AND RECOIL CORRECTIONS

In addition to the effects of relativity and electron correlation, further physical effects have to be considered for a complete description of energy levels. These are discussed in the following.

A. QED corrections

QED effects give sizeable shifts in the absolute values of dielectronic recombination resonances. For single-particle orbitals (hydrogen-like systems), the self-energy (SE), which is the dominant radiative correction to the energy level [34], can be expressed in terms of a scaled function $F_{n\kappa}(Z\alpha)$ which reads (in atomic units)

$$E_{n\kappa}^{\mathrm{SE}} = \frac{Z^4}{\pi c^3 n^3} F_{n\kappa}(Z\alpha). \tag{17}$$

Tabulations of this function are given in the literature for a wide range of nuclear charges and electronic states [35–40], including nuclear size corrections [41]. In our MCDF and CI-DFS calculations, the screening of the SE in many-electron states is approximated by assigning an effective nuclear charge $Z_{n\kappa}^{\mathrm{eff}}$ to each electronic orbital. These effective nuclear charges are determined by matching the electron density resulting from the DF self-consistent procedure to the density of the corresponding hydrogenic orbital at a Compton wavelength distance from the origin.

The MCDF results are corrected for self-energy screening effects in the following way: For each one-electron orbital, Eq. (17)is rescaled as

$$E_{n\kappa}^{\mathrm{SE,appr.}} = q_{n\kappa}^{\mathrm{eff}} \frac{Z(Z_{n\kappa}^{\mathrm{eff}})^3}{\pi c^3 n^3} F_{n\kappa}(Z\alpha) \tag{18}$$

with the effective occupation $q_{n\kappa}^{\mathrm{eff}}$ of a given subshell $n\kappa$ defined in terms of the physical configuration occupation num-

TABLE VIII. Quantum electrodynamic contributions to the initial and intermediate level energies corresponding to *KLL* DR into He-like Hg (units are eV).

		QED screening	
State	QED	MCDF	CI-DFS
$[1s^2]_0$	326.0(1)	−4.04(0.6)	−4.35(0.6)
$[1s2s^2]_{1/2}$	219.8(1)	−4.76(1.7)	−5.61(1.7)
$[(1s2s)_0 2p_{1/2}]_{1/2}$	193.8(1)	−3.56(2.9)	−2.12(2.9)
$[(1s2p_{1/2})_0 2p_{3/2}]_{3/2}$	196.0(1)	−3.36(2.4)	−2.19(2.4)
$[(1s2s)_0 2p_{3/2}]_{3/2}$	169.9(1)	−0.61(0.4)	−0.83(0.4)
$[1s(2p_{3/2})_2^2]_{5/2}$	172.1(1)	−0.60(0.6)	−0.90(0.6)

TABLE IX. Quantum electrodynamic contributions to the initial and intermediate level energies corresponding to *KLL* DR into Li-like Hg (units are eV).

		QED screening	
State	QED	MCDF	CI-DFS
$[1s^2 2s]_{1/2}$	354.4(1)	−6.32(1.2)	−6.90(1.2)
$[1s2s^2 2p_{1/2}]_1$	222.2(1)	−3.92(1.0)	−4.37(1.0)
$[((1s2s)_1 2p_{1/2})_{3/2} 2p_{3/2}]_2$	198.4(1)	−2.32(1.4)	−3.08(1.4)
$[((1s2s)_1 2p_{1/2})_{3/2} 2p_{3/2}]_1$	198.4(1)	−2.31(1.4)	−3.08(1.4)
$[((1s2s)_0 2p_{1/2})_{1/2} 2p_{3/2}]_2$	198.4(1)	−4.03(2.0)	−3.08(2.0)
$[((1s2s)_1 2p_{1/2})_{3/2} 2p_{3/2}]_3$	198.4(1)	−2.32(1.4)	−3.07(1.4)
$[(1s2s)_1 (2p_{3/2})_2^2]_3$	200.5(1)	−2.68(1.0)	−3.17(1.0)

TABLE X. Quantum electrodynamic contributions to the initial and intermediate level energies corresponding to *KLL* DR into Be-like Hg (units are eV).

		QED screening	
State	QED	MCDF	CI-DFS
$[1s^2 2s^2]_0$	382.8(1)	−9.37(3.4)	−11.11(3.4)
$[1s2s^2 (2p_{1/2})^2]_{1/2}$	224.6(1)	−4.91(1.6)	−5.68(1.6)
$[(1s2s^2 2p_{1/2})_1 2p_{3/2}]_{3/2}$	226.8(1)	−4.76(2.1)	−5.79(2.1)
$[(1s2s^2 2p_{1/2})_0 2p_{3/2}]_{3/2}$	226.8(1)	−4.79(2.1)	−5.79(2.1)
$[(1s2s^2 2p_{1/2})_1 2p_{3/2}]_{5/2}$	226.8(1)	−4.88(1.8)	−5.79(1.8)
$[1s2s^2 (2p_{3/2})_2^2]_{5/2}$	228.9(1)	−5.59(2.3)	−6.72(2.3)

TABLE XI. Quantum electrodynamic contributions to the initial and intermediate level energies corresponding to *KLL* DR into B-like Hg (units are eV).

		QED screening	
State	QED	MCDF	CI-DFS
$[1s^22s^22p_{1/2}]_{1/2}$	385.2(1)	−10.05(3.6)	−11.87(3.6)
$[1s2s^2(2p_{1/2})^22p_{3/2}]_1$	229.2(1)	−5.33(3.6)	−7.17(3.6)
$[1s2s^2(2p_{1/2})^22p_{3/2}]_2$	229.2(1)	−5.39(3.6)	−7.17(3.6)
$[(1s2s^22p_{1/2})_1(2p_{3/2})_2^2]_3$	231.3(1)	−6.77(1.1)	−7.31(1.1)

bers $q_{n\kappa,k}$, summed over the entire set of configuration state functions used:

$$q_{n\kappa}^{\mathrm{eff}} = \sum_{k=1}^{n_c} c_k^2 q_{n\kappa,k}. \tag{19}$$

In this way, the configuration mixing of the SE screening corrections is approximately accounted for, and this effect is relevant for the excited states studied here.

As an example, we would like to mention that the SE screening result obtained using this procedure in the case of the MCDF method is −5.13 eV for the ground state of He-like Hg, which has to be compared to the result of −5.9289(1) eV obtained using *ab initio* calculations based on the direct evaluation of the screening Feynman diagrams in Ref. [31]. Furthermore, our SE screening estimate of −11.17 eV for the Be-like ground state configuration is comparable to the estimate value of −10.69 eV from Ref. [42], based on the Welton model, and the value of −9.78 eV of Ref. [43], in which the effect of the electron-electron interactions is treated as a first-order perturbation to the self-energy by an effective screening potential. The reasonable agreement of these results in the case of the He- and Be-like ground state configurations encourages us to apply our approximate scheme to more complex many-electron states where *ab initio* calculations are neither available nor feasible yet. Note that this procedure differs from the one applied in Ref. [19]and, according to our experience, yields results in better agreement with rigorous QED calculations.

The vacuum polarization (VP) correction describes the short-range modification of the nuclear field due to screening by virtual electron-positron pairs. Expressions for VP potentials have been given in the literature, e.g., in Ref. [44], and its matrix elements can easily be calculated by numerical integration. The matrix elements of the VP corrections are then added to the matrix elements of H^{DC}. The Wichmann-Kroll corrections to the one-loop VP diagram are taken from Ref. [35]. Our values agree well with the accurate QED-based calculations for the ground state in He-like Hg ions. The VP screening correction calculated with MCDF wave functions is, e.g., 1.09 eV, which is to be compared to the precise result of 1.2980(2) eV from Ref. [31].

In order to allow for a meaningful comparison, a *slightly different* procedure is applied to correct the CI-DFS results for radiative effects (as opposed to the MCDF results). The effective nuclear charge of each subshell orbital, matched at a Compton wavelength distance from the nucleus, is used to interpolate the one-electron QED corrections given for integer Z values in Ref. [35]. These results are also multiplied with effective occupation numbers as described above.

Tables VIII–XIshow the results of these calculational schemes. The errors of the one-electron QED contributions are taken from the literature and are negligible in our case. As the two SCF theories (MCDF and CI-DFS) use different approximate methods to evaluate QED screening contributions, twice the difference of the two results is taken as an error estimate for both theories. This estimate is motivated by the following consideration: for the ground state of He-like Hg, a precise value of the QED screening is given in a recent article [31]as −4.6309(2) eV. The result of the CI-DFS-theory estimate is −4.35 eV; the above-mentioned method used to estimate screening corrections to MCDF energies yields −4.04 eV. In the case of the CI-DFS calculations, this is the most prominent source of the total error of the resonance energies. In the case of the MCDF results, the errors associated to Coulomb correlation and Breit contributions are, in some cases, of the same magnitude.

Within the QMB approach and in the first order of the interelectronic interaction, the screening of the Lamb shift can be described by the screened self-energy (SSE) and screened vacuum polarization (SVP) diagrams. The SVP diagrams can be taken into account relatively easily. They can be evaluated in all orders in αZ by the inclusion of the vacuum polarization potential into the initial Hamiltonian. However, the *ab initio* calculation of the SSE diagrams requires much more effort in the many-electron case. Since the

TABLE XII. Finite nuclear mass contributions to the initial and intermediate state level energies E_i, E_d for initially He-like Hg ions (units are eV).

	NMS		RNMS	SMS		RSMS
State	MCDF	CI-DFS	CI-DFS	MCDF	CI-DFS	CI-DFS
$[1s^2]_0$	0.635(02)	0.634(02)	−0.186(30)	0.001(01)	0.002(01)	−0.001(1)
$[1s2s^2]_{1/2}$	0.489(04)	0.487(04)	−0.138(30)	−0.001(01)	−0.002(01)	0.001(1)
$[(1s2s)_02p_{1/2}]_{1/2}$	0.486(02)	0.485(02)	−0.136(30)	−0.030(10)	−0.035(10)	0.022(1)
$[(1s2p_{1/2})_02p_{3/2}]_{3/2}$	0.465(02)	0.464(02)	−0.120(30)	−0.031(10)	−0.027(10)	0.006(1)
$[(1s2s)_02p_{3/2}]_{3/2}$	0.464(02)	0.464(02)	−0.118(30)	−0.020(50)	−0.045(50)	0.029(1)
$[1s(2p_{3/2})_2^2]_{5/2}$	0.431(20)	0.443(20)	−0.102(30)	−0.076(12)	−0.064(12)	0.014(1)

TABLE XIII. Finite nuclear mass contributions to the initial and intermediate state level energies E_i, E_d for initially Li-like Hg ions (units are eV).

	NMS		RNMS	SMS		RSMS
State	MCDF	CI-DFS	CI-DFS	MCDF	CI-DFS	CI-DFS
$[1s^22s]_{1/2}$	0.717(4)	0.715(4)	−0.208(30)	0.001(01)	0.003(01)	−0.001(1)
$[1s2s^22p_{1/2}]_1$	0.568(2)	0.568(2)	−0.157(30)	−0.021(04)	−0.019(04)	0.012(1)
$[((1s2s)_1 2p_{1/2})_{3/2}2p_{3/2}]_2$	0.545(2)	0.546(2)	−0.140(30)	−0.024(18)	−0.033(18)	0.018(1)
$[((1s2s)_1 2p_{1/2})_{3/2}2p_{3/2}]_1$	0.548(6)	0.545(6)	−0.140(30)	−0.016(02)	−0.016(02)	0.014(1)
$[((1s2s)_0 2p_{1/2})_{1/2}2p_{3/2}]_2$	0.547(6)	0.544(6)	−0.139(30)	−0.055(06)	−0.052(06)	0.024(1)
$[((1s2s)_1 2p_{1/2})_{3/2}2p_{3/2}]_3$	0.546(2)	0.546(2)	−0.140(30)	−0.059(02)	−0.059(02)	0.020(1)
$[(1s2s)_1(2p_{3/2})_2^2]_3$	0.525(2)	0.525(2)	−0.124(30)	−0.063(02)	−0.063(02)	0.013(1)

SSE and SVP contributions are of the same order and have opposite signs, we preferred in the present calculation to neglect both these corrections within QMB. Their calculation is possible in principle, but is expected to be much more time consuming than the evaluations of the terms considered so far.

In our present QMB calculations, the one-electron one-loop SE and VP terms are calculated as described in, e.g., Ref. [31]. It was not our aim to reach a very high precision for the values of the energy levels, but we rather tried to demonstrate that this method can in principle be applied to the description of such complicated states involved in the dielectronic excitation process. Therefore we neglected two-loop QED effects and the contributions caused by the screening of the Lamb shift. As the approximate screening corrections to level energies (Tables VIII–XI) are in the range of 1–12 eV, the largest uncertainty of the QMB theoretical result arises from omitting the latter terms.

B. Nuclear recoil corrections

For our investigation, it turns out that radiative-recoil corrections are completely negligible on the level of the experimental precision, and an approximate treatment of the nuclear recoil effect on the level of nuclear finite-mass shifts is sufficient. Still it is important to generalize the normal mass shift (NMS) and the specific mass shift (SMS) correction to the relativistic case. The relativistic one-particle operator of the normal mass shift contribution is given by[45–47]

$$H_{\mathrm{NMS}} = \frac{1}{2M_{\mathrm{nuc}}} \sum_{i=1}^{N} \left[\mathbf{p}_i^2 - \frac{Z}{r_i} \left(\boldsymbol{\alpha}_i + \frac{(\boldsymbol{\alpha}_i \cdot \mathbf{r}_i)\mathbf{r}_i}{r_i^2} \right) \cdot \mathbf{p}_i \right], \quad (20)$$

with M_{nuc} being the nuclear mass calculated from the atomic masses given in Table Iby subtracting the total electron mass corresponding to the ground state of the neutral atom. We find that, due to the large nuclear masses of the heavy ion systems studied here, the normal mass shift contribution is negligible for our investigation. The second term in Eq. (20)describes the relativistic operator correction (RNMS) to the nuclear recoil effect.

The correction due to the correlated motion of the electrons (SMS) is described by the following relativistic two-particle operator [45–47]:

$$H_{\mathrm{SMS}} = \frac{1}{M_{\mathrm{nuc}}} \sum_{i<j}^{N} \left[\mathbf{p}_i \cdot \mathbf{p}_j - \frac{Z}{r_i} \left(\boldsymbol{\alpha}_i + \frac{(\boldsymbol{\alpha}_i \cdot \mathbf{r}_i)\mathbf{r}_i}{r_i^2} \right) \cdot \mathbf{p}_j \right]. \quad (21)$$

Here, we introduce the notation RSMS for the relativistic correction (second term in the parentheses). For an application of the relativistic recoil operator corrections, see, e.g., Ref. [26]. The corrections were found to be essential for an evaluation of nuclear recoil corrections in relativistic systems. (In typical cases, the application of the nonrelativistic

TABLE XIV. Finite nuclear mass contributions to the initial and intermediate state level energies E_i, E_d for initially Be-like Hg ions (units are eV).

	NMS		RNMS	SMS		RSMS
State	MCDF	CI-DFS	CI-DFS	MCDF	CI-DFS	CI-DFS
$[1s^22s^2]_0$	0.798(4)	0.796(4)	−0.228(30)	0.000(01)	0.001(01)	−0.001(1)
$[1s2s^2(2p_{1/2})^2]_{1/2}$	0.647(2)	0.646(2)	−0.176(30)	−0.060(06)	−0.057(06)	0.035(1)
$[(1s2s^22p_{1/2})_1 2p_{3/2}]_{3/2}$	0.626(2)	0.625(2)	−0.160(30)	−0.085(60)	−0.057(60)	0.023(1)
$[(1s2s^22p_{1/2})_0 2p_{3/2}]_{3/2}$	0.626(2)	0.627(2)	−0.161(30)	−0.020(50)	−0.044(50)	0.028(1)
$[(1s2s^22p_{1/2})_1 2p_{3/2}]_{5/2}$	0.626(2)	0.626(2)	−0.160(30)	−0.059(04)	−0.057(04)	0.020(1)
$[1s2s^2(2p_{3/2})_2^2]_{5/2}$	0.605(2)	0.604(2)	−0.145(30)	−0.064(02)	−0.063(02)	0.013(1)

TABLE XV. Finite nuclear mass contributions to the initial and intermediate state level energies E_i, E_d for initially B-like Hg ions (units are eV).

	NMS		RNMS	SMS		RSMS
State	MCDF	CI-DFS	CI-DFS	MCDF	CI-DFS	CI-DFS
$[1s^22s^22p_{1/2}]_{1/2}$	0.876(4)	0.874(4)	−0.247(30)	−0.055(4)	−0.053(4)	0.032(1)
$[1s2s^2(2p_{1/2})^22p_{3/2}]_1$	0.704(4)	0.702(4)	−0.179(30)	−0.047(8)	−0.043(8)	0.031(1)
$[1s2s^2(2p_{1/2})^22p_{3/2}]_2$	0.704(2)	0.703(2)	−0.179(30)	−0.097(6)	−0.094(6)	0.043(1)
$[(1s2s^22p_{1/2})_1(2p_{3/2})_2^2]_3$	0.683(2)	0.682(2)	−0.164(30)	−0.083(4)	−0.081(4)	0.025(1)

NMS and SMS operators to Dirac wave functions strongly overestimates the relativistic correction to the recoil corrections.)

Tables XII–XVcontain numerical results for the recoil corrections to all states of relevance for our investigation in He-, Li-, Be-, and B-like Hg ions. The errors are determined by multiplying the difference of the CI-DFS and MCDF results by a factor of 2. The same holds for the specific mass shift term. The relativistic correction terms to the NMS and SMS operators are only calculated in the framework of the CI-DFS theory; to these results, an error of 0.03 eV (RNMS) and 0.001 eV (RSMS) is assigned. As these terms are not included in the results of the MCDF method, a partial error corresponding to the largest contribution from the CI-DFS theory (rounded up) is assigned to the final MCDF result.

As is evident from Tables XII–XV, the nuclear mass shift corrections to *KLL* resonance energies in Hg ions are on the level of only 1 eV and thus not decisive at the present level of the experimental accuracies. Nuclear mass effects are clearly dominated by finite nuclear size contributions. The hyperfine interaction between the nucleus and the electron and the nuclear polarization contribution is not taken into account in the present work. Specifically, the results in Refs. [48,49]for the nuclear polarization term in even-A actinide nuclei can be used to infer that for elements as heavy as Hg, this effect gives a correction to the resonance transition energies in the order of 0.1 eV and can be regarded as negligible. The hyperfine splitting of *KLL* DR resonance peaks can be assumed to be dominated by the splitting of the $1s$ one-electron orbital, which is calculated to be 0.954 28 and 0.703 03 eV for the isotopes ^{199}Hg and ^{201}Hg with nonvanishing nuclear spins, respectively [50]. This introduces a slight line broadening to the experimental spectra as the hyperfine levels cannot be resolved currently. Assuming a statistical population of the hyperfine states, the shift of the DR resonance peaks due to hyperfine interactions can be neglected.

IV. THEORETICAL RESONANCE ENERGIES AND COMPARISON WITH EXPERIMENT

In this section, we compare our total values and their corresponding theoretical errors for the resonance transition energies with experimental data taken from the companion paper [12]. The partial uncertainties associated to specific energy corrections, evaluated as discussed in the previous sections, are added quadratically for ground states as well as for the autoionizing intermediate states involved in the dielectronic recombination process. These errors are rounded up to yield an error given as an integer in eV. For an approximation of the error of resonance transition energies (i.e., the differences of the autoionizing state to the ground state energy), these uncertainties are again added quadratically and rounded up to an integer value in units of eV.

Finally, Table XVIcontains *KLL* DR resonance energies for initially He-, Li-, Be-, and B-like ions obtained from different theoretical approaches, as described in Sec. II, and our experimental results. The values given in Table XVIare equivalent to those in Table I of Ref. [12]. We recall them here, supplementing theoretical error estimates (note that the method referred to as MCDF_M in [12]is simply called MCDF in the current study). In Table XVI, the notation $[i]_J$ is used for the initial ground state of the ion and $[d]_J$ denotes the intermediate state of the recombination process. It should be stressed again here that all experimental resonance energies are pinned to the theoretical value of 46.358 keV of the $[1s2s^2]_{1/2}$ resonance energy to reduce experimental uncertainties (see Ref. [12]). Therefore, when comparing experimental and theoretical results, it is more meaningful to refer the measured energies to the $[1s2s^2]_{1/2}$ value of each individual calculation.

The resonance energies show a good agreement with experimental results, especially in the case of initially He-like ions. This can be explained by the simpler electronic structure of the He-like ground state and the Li-like *KLL* autoionizing states.

A particularly interesting case is provided by DR resonances in initially Li-like ions, with intermediate states $[((1s2s)_12p_{1/2})_{3/2}2p_{3/2}]_2$ and $[((1s2s)_12p_{1/2})_{3/2}2p_{3/2}]_1$. Discrepancies of theory and experiment amount to as much as 24 eV (QMB). The disagreements decrease significantly in the case of MCDF results. However, the MCDF resonance energies are associated with larger uncertainties than those of the CI-DFS results due to the relatively poor convergence of the MCDF expansion in this special case. The largest scatter of theoretical values is also observed for these two resonances.

For the case of initially Be-like Hg ions, theoretical and experimental error bars overlap, and the CI-DFS and the MCDF results show the smallest average deviations for the experimental data. The discrepancy of the QMB results can be associated to the QED screening and higher-order retardation contributions, which were not calculated within the

TABLE XVI. Theoretical and experimental *KLL* DR resonance energies for He-, Li-, Be- and B-like Hg ions (here, units are keV). A value of 46.358 keV of the $[1s2s^2]_{1/2}$ resonance energy is used as a reference for the experimental energy scale (see text).

$[i]_J$	$[d]_J$	Experiment	MCDF	CI-DFS	QMB
$[1s^2]_0$	$[1s2s^2]_{1/2}$	46.358(4)	46.362(3)	46.361(3)	46.359
$[1s^2]_0$	$[(1s2s)_0 2p_{1/2}]_{1/2}$	46.611(6)	46.614(5)	46.614(4)	46.612
$[1s^2]_0$	$[(1s2s)_0 2p_{3/2}]_{3/2}$	48.844(6)	48.842(5)	48.843(4)	48.840
$[1s^2]_0$	$[(1s2p_{1/2})_0 2p_{3/2}]_{3/2}$	48.918(9)	48.926(3)	48.926(2)	48.922
$[1s^2]_0$	$[(1s2s)_0 2p_{3/2}]_{3/2}$	48.845(5)	48.842(5)	48.843(4)	48.840
$[1s^2]_0$	$[1s(2p_{3/2})^2_2]_{5/2}$	51.064(6)	51.065(3)	51.064(2)	51.058
$[1s^22s]_{1/2}$	$[1s2s^22p_{1/2}]_1$	46.686(5)	46.688(4)	46.690(3)	46.686
$[1s^22s]_{1/2}$	$[((1s2s)_1 2p_{1/2})_{3/2} 2p_{3/2}]_2$	49.086(6)	49.077(9)	49.067(3)	49.063
$[1s^22s]_{1/2}$	$[((1s2s)_1 2p_{1/2})_{3/2} 2p_{3/2}]_1$	49.136(9)	49.126(9)	49.118(3)	49.113
$[1s^22s]_{1/2}$	$[((1s2s)_0 2p_{1/2})_{1/2} 2p_{3/2}]_2$	49.218(13)	49.215(5)	49.214(4)	49.209
$[1s^22s]_{1/2}$	$[((1s2s)_1 2p_{1/2})_{3/2} 2p_{3/2}]_3$	48.970(5)	48.971(5)	48.966(3)	48.961
$[1s^22s]_{1/2}$	$[(1s2s)_1 (2p_{3/2})^2_2]_3$	51.154(5)	51.155(4)	51.153(3)	51.147
$[1s^22s^2]_0$	$[1s2s^2(2p_{1/2})^2]_{1/2}$	47.135(5)	47.134(5)	47.135(5)	47.121
$[1s^22s^2]_0$	$[(1s2s^22p_{1/2})_1 2p_{3/2}]_{3/2}$	49.270(8)	49.260(6)	49.260(5)	49.251
$[1s^22s^2]_0$	$[(1s2s^22p_{1/2})_0 2p_{3/2}]_{3/2}$	49.349(6)	49.346(5)	49.347(5)	49.333
$[1s^22s^2]_0$	$[(1s2s^22p_{1/2})_1 2p_{3/2}]_{5/2}$	49.265(17)	49.253(6)	49.254(6)	49.246
$[1s^22s^2]_0$	$[1s2s^2(2p_{3/2})^2_2]_{5/2}$	51.433(6)	51.430(6)	51.429(5)	51.423
$[1s^22s^22p_{1/2}]_{1/2}$	$[1s2s^2(2p_{1/2})^2 2p_{3/2}]_1$	49.557(4)	49.553(8)	49.551(8)	49.546
$[1s^22s^22p_{1/2}]_{1/2}$	$[1s2s^2(2p_{1/2})^2 2p_{3/2}]_2$	49.499(4)	49.493(8)	49.493(8)	49.487
$[1s^22s^22p_{1/2}]_{1/2}$	$[1s2s^2(2p_{1/2})^2 2p_{3/2}]_1$	49.552(7)	49.553(8)	49.551(8)	49.546
$[1s^22s^22p_{1/2}]_{1/2}$	$[(1s2s^22p_{1/2})_1 (2p_{3/2})^2_2]_3$	51.603(8)	51.598(7)	51.603(7)	51.593

current proof-of-principle study regarding the basic applicability of the QMB approach to many-electron systems. It is interesting to observe, however, an apparent trend in all theories to predict lower resonance energies for recombination into Be-like Hg ions than the experimental results, rather than showing a scatter around the measured data. For initially B-like Hg ions, theoretical and experimental error bars again overlap. It might also be interesting to note that, for the B-like case, the same uncertainties have to be assigned to MCDF and CI-DFS theoretical values due to large common errors of the QED screening contributions.

The overall tendency of the final uncertainties of MCDF and CI-DFS resonance energies is summarized as follows: they increase with the number of electrons, as expected, because the uncertainties of the Coulomb and Breit contributions become larger as well as uncertainties associated to the QED screening approximations. The total CI-DFS uncertainties are usually a few eV smaller than the errors of the MCDF method. The overall stronger disagreement of the QMB results supports the conclusion that QED screening terms and higher-order retardation corrections may have to be taken into account more rigorously in future calculations, if one would like to apply the QMB method to complex many-electron states as the ones studied here.

V. SUMMARY

The central point of this article has been the process of dielectronic recombination via *KLL* resonant channels. We have analyzed in detail various effects which contribute to the resonance energies observed in DR into He-, Li-, Be-, and B-like Hg ions. We applied the MCDF, CI-DFS, and QMB methods to determine atomic state functions and energies. Our calculations include Coulomb correlation and Breit contributions, approximations for the many-electron QED terms, and finite nuclear size as well as recoil corrections. The comparison of our theoretical values with the experimental data shows a good overall agreement.

The main results of the current investigation are as follows: In Tables IV–VII, we report Coulomb and Breit contributions for ground states and autoionizing states involved in the experimentally resolved resonance transitions, calculated in the framework of the MCDF and CI-DFS schemes. Frequency-dependent retardation contributions to the electron-electron interaction are calculated as a first-order perturbation. In the subsequent Tables VIII–XI, results of two different semi-empirical methods to estimate electron screening effects on QED corrections are listed and compared. Nuclear recoil contributions, including relativistic operator corrections, are presented in Tables XII–XV. Our final resonance energy results, calculated by means of the MCDF, CI-DFS, and QMB methods, are summarized in Table XVIand are compared to our experimental data.

Due to the complex nature of the physical problem, results in many-body theories are commonly provided without error estimates in the literature (see, e.g., [51]). In this article we assigned theoretical uncertainties to each of the consid-

ered contributions and analyzed their respective relevance in interpreting the experimental results. On the theoretical side, the largest error bars are due to QED screening effects and higher-order retardation contributions. As electron interaction contributions to dielectronic resonance energies beyond the no-pair approximation may not be negligible in the case of heavy ions, the calculation of such terms is necessary in the future to improve the accuracy of theoretical results. On the experimental side, the least satisfactory agreement of theory and experiment for $[((1s2s)_1 2p_{1/2})_{3/2} 2p_{3/2}]_2$ and $[((1s2s)_1 2p_{1/2})_{3/2} 2p_{3/2}]_1$ intermediate states originating from recombination into initially Li-like ions suggests further studies along the isoelectronic sequence, with a special emphasis on these resonances. These further investigations might help to resolve the causes of interesting discrepancies, which are still present for specific resonances, and to gain more insight into the structure and dynamics of relativistic multiply-excited few-electron states.

ACKNOWLEDGMENTS

A.N.A. and I.I.T. would like to thank the Max-Planck-Institut für Kernphysik (Heidelberg) for the hospitality and excellent working conditions during their stay there. A.N.A. acknowledges support from the "Dynasty" foundation and I.I.T. from the Russian Foundation for Basic Research (Grant Nos. 04-02-17574 and 05-03-32585). U.D.J. acknowledges support from the Deutsche Forschungsgemeinschaft (Heisenberg program).

[1] H. F. Beyer and V. P. Shevelko, *Introduction to the Physics of Highly Charged Ions* (IOP, Bristol, 2002).
[2] *An International Accelerator Facility for Beams of Ions and Antiprotons, Conceptual Design Report*, edited by H. H. Gutbrod, K.-D. Gross, W. F. Henning, and V. Metag (GSI, Darmstadt, 2001).
[3] P. Beiersdorfer, A. L. Osterheld, J. H. Scofield, J. R. Crespo López-Urrutia, and K. Widmann, Phys. Rev. Lett. **80**, 3022 (1998).
[4] C. Brandau *et al.*, Phys. Rev. Lett. **91**, 073202 (2003).
[5] P. Beiersdorfer, H. Chen, D. B. Thorn, and E. Träbert, Phys. Rev. Lett. **95**, 233003 (2005).
[6] A. Wolf *et al.*, Nucl. Instrum. Methods Phys. Res. A **441**, 183 (2000).
[7] A. Müller and S. Schippers, ASP Conf. Ser. **247**, 53 (2001).
[8] D. A. Knapp, Z. Phys. D: At., Mol. Clusters **21**, 143 (1991).
[9] A. J. González Martínez *et al.*, Phys. Rev. Lett. **94**, 203201 (2005).
[10] Y. Zou, J. R. Crespo López-Urrutia, and J. Ullrich, Phys. Rev. A **67**, 042703 (2003).
[11] R. Schuch, E. Lindroth, S. Madzunkov, M. Fogle, T. Mohamed, and P. Indelicato, Phys. Rev. Lett. **95**, 183003 (2005).
[12] A. J. González Martínez *et al.*, Phys. Rev. A **73**, 052710 (2006).
[13] A. J. González Martínez, Ph.D. thesis, Ruperto-Carola University of Heidelberg, Germany (2005).
[14] I. P. Grant, Adv. Phys. **19**, 747 (1970).
[15] J. P. Desclaux, D. F. Mayers, and F. O'Brien, J. Phys. B **4**, 631 (1971).
[16] I. P. Grant, Comput. Phys. Commun. **17**, 149 (1979).
[17] I. P. Grant, *Relativistic Effects in Atoms and Molecules* (Plenum, New York, 1988), Vol. 2, pp. 1–71.
[18] K. G. Dyall, I. P. Grant, C. T. Johnson, F. A. Parpia, and E. P. Plummer, Comput. Phys. Commun. **55**, 425 (1989).
[19] F. A. Parpia, C. Froese Fischer, and I. P. Grant, Comput. Phys. Commun. **94**, 249 (1996).
[20] S. Zakowicz, Z. Harman, N. Grün, and W. Scheid, Phys. Rev. A **68**, 042711 (2003).
[21] M. S. Pindzola, F. J. Robicheaux, N. R. Badnell, M. H. Chen, and M. Zimmermann, Phys. Rev. A **52**, 420 (1995).
[22] C. Brandau *et al.*, Phys. Rev. Lett. **89**, 053201 (2002).
[23] I. Draganić, J. R. Crespo López-Urrutia, R. DuBois, S. Fritzsche, V. M. Shabaev, R. Soria Orts, I. I. Tupitsyn, Y. Zou, and J. Ullrich, Phys. Rev. Lett. **91**, 183001 (2003).
[24] A. Lapierre *et al.*, Phys. Rev. Lett. **95**, 183001 (2005).
[25] I. I. Tupitsyn, A. V. Volotka, D. A. Glazov, V. M. Shabaev, G. Plunien, J. R. Crespo López-Urrutia, A. Lapierre, and J. Ullrich, Phys. Rev. A **72**, 062503 (2005).
[26] I. I. Tupitsyn, V. M. Shabaev, J. R. Crespo López-Urrutia, I. Draganić, R. Soria Orts, and J. Ullrich, Phys. Rev. A **68**, 022511 (2003).
[27] I. Angeli, At. Data Nucl. Data Tables **87**, 185 (2004).
[28] A. H. Wapstra, G. Audi, and C. Thibault, At. Data Nucl. Data Tables **729**, 129 (2003).
[29] A. H. Wapstra, G. Audi, and C. Thibault, At. Data Nucl. Data Tables **729**, 337 (2003).
[30] A. N. Artemyev, V. M. Shabaev, M. M. Sysak, V. A. Yerokhin, T. Beier, G. Plunien, and G. Soff, Phys. Rev. A **67**, 062506 (2003).
[31] A. N. Artemyev, V. M. Shabaev, V. A. Yerokhin, G. Plunien, and G. Soff, Phys. Rev. A **71**, 062104 (2005).
[32] V. M. Shabaev, Phys. Rep. **356**, 119 (2002).
[33] W. R. Johnson, S. A. Blundell, and J. Sapirstein, Phys. Rev. A **37**, 307 (1988).
[34] P. J. Mohr, Ann. Phys. (N.Y.) **8**, 26 (1974).
[35] W. R. Johnson and G. Soff, At. Data Nucl. Data Tables **33**, 405 (1985).
[36] P. J. Mohr and Y.-K. Kim, Phys. Rev. A **45**, 2727 (1992).
[37] P. J. Mohr, Phys. Rev. A **46**, 4421 (1992).
[38] U. D. Jentschura, P. J. Mohr, and G. Soff, Phys. Rev. A **63**, 042512 (2001).
[39] E.-O. Le Bigot, P. Indelicato, and P. J. Mohr, Phys. Rev. A **64**, 052508 (2001).
[40] U. D. Jentschura and P. J. Mohr, Phys. Rev. A **69**, 064103 (2004).
[41] P. J. Mohr and G. Soff, Phys. Rev. Lett. **70**, 158 (1993).
[42] J. P. Santos, G. C. Rodrigues, J. P. Marques, F. Parente, J. P. Desclaux, and P. Indelicato, Eur. Phys. J. D **37**, 201 (2006).
[43] P. Indelicato and P. J. Mohr, Phys. Rev. A **63**, 052507 (2001).
[44] L. W. Fullerton and G. A. Rinker, Phys. Rev. A **13**, 1283

(1976).
[45] V. M. Shabaev, Teor. Mat. Fiz. **63**, 394 (1985).
[46] V. M. Shabaev, Yad. Fiz. **47**, 107 (1988).
[47] C. W. Palmer, J. Phys. B **20**, 5987 (1987).
[48] G. Plunien and G. Soff, Phys. Rev. A **51**, 1119 (1995).
[49] G. Plunien and G. Soff, Phys. Rev. A **53**, 4614(E) (1996).
[50] S. Boucard and P. Indelicato, Eur. Phys. J. D **8**, 59 (2000).
[51] W. R. Johnson, D. R. Plante, and J. Sapirstein, Adv. At., Mol., Opt. Phys. **35**, 255 (1995).